Elastic response of cross laminated engineered bamboo panels subjected to in-plane loading.

Hector F. Archila, Ph. D., PGDPM, BArch
Amphibia BASE Ltd, Bath, UK & Department of Architecture and Civil Engineering, University of Bath, Bath, UK.
Corresponding author: hector.archila@bath.edu

Andrew Rhead, MSci(Mmath) PhD
Department of Mechanical Engineering, University of Bath, Bath, UK.

Martin P. Ansell, BSc PhD FIMMM
Department of Mechanical Engineering, University of Bath, Bath, UK.

Pete Walker, BSc, PhD, MIEAust, CPEng, MICE, CEng
Department of Architecture and Civil Engineering, University of Bath, Bath, UK.

Juan Lizarazo-Marriaga, PhD, MSc
Departamento Ingeniería Civil y Agrícola, Grupo de Investigación en Análisis, Diseño y Materiales GIES. Universidad Nacional de Bogotá, Bogotá, UK

Abstract

Novel cross-laminated bamboo panels comprising three and five layers (G-XLam3 and G-XLam 5) were tested in compression along the main (0º) and the transverse (90º) direction. Linear variable displacement transducer (LVDT) and non-contact 3D digital image correlation (DIC) measuring techniques were used separately to measure deformation in the elastic region and the elastic moduli $Ep_{C,0}$ and $Ep_{C,90}$ were derived. Mean elastic modulus values obtained using LVDTs exhibited a good match with analytically predicted values. By contrast, elastic values obtained by the DIC method were considerably higher and presented a considerable scatter of results. For instance, $Ep_{C,0}$ for G-XLam3 and G-XLam5 panels were 17.22GPa and 15.67Gpa and 14.86GPa and 12.48GPa, from DIC and LVDT respectively. In general, G-XLam panels with a fifth of the cross-sectional thickness and twice the density of analogous cross-laminated timber (CLT) exhibited an approximate two-fold increase in $Ep_{C,0}$ and $Ep_{C,90}$. Overall, this research provides guidelines for the assessment and standardisation of testing procedures for similar engineered bamboo products (EBPs) using contact and non-contact methods and highlights the potential of using G-XLam panels in stiffness driven applications and in combination with wood for structural purposes.

Keywords chosen from ICE Publishing list

Bamboo, engineered bamboo products, cross laminated panels; digital image correlation (DIC); non-contact optical technique; optical metrology; full field deformation method. **From ICE Proceedings - journal keyword list**: Materials technology, Strength & testing of materials

List of notation (examples below)

Ɛ	engineering strain
X_1	geometric axis corresponding to the longitudinal (L) orientation
X_2	geometric axis corresponding to the tangential (T) orientation
X_3	geometric axis corresponding to the radial (R) orientation
L	length
ΔL	change in length in unit of original length
l_0	initial length of the extensometer
l_1	final length of the extensometer
l	gauge length (A-B length of the virtual extensometer)
t	panel thickness
A	cross sectional area of the panel
F_{max}	maximum permitted load
$E_{C,0}$	compression moduli of elasticity of the panels in the longitudinal direction
$E_{C,90}$	compression moduli of elasticity of the panels in the transverse direction
λ	slenderness ratio
ρ	density

Introduction

The species of bamboo *Guadua angustifolia* Kunth (Guadua) has been widely used for structural applications in small and large-scale buildings, bridges and temporary structures in South and Central America (Jayanetti & Follett 1998; Janssen 2000; Hidalgo-López 2003; Villegas 2003; van der Lugt et al. 2009; Xiao et al. 2008; Minke 2012; Archila et al. 2012; Trujillo et al. 2013). In addition to its large availability and low cost, the overall low weight, moderate ductility and high strength of traditional Guadua building systems has been key for its utilization in this earthquake-prone region (Kaminski et al. 2016). Guadua's high biomass production, renewability and high strength to weight ratio make it a potential material for mainstream applications in the construction industry. However, Guadua remains a material for predominantly vernacular construction associated with high levels of manual labour and structural unpredictability (Archila et al. 2012). Additionally, issues regarding poor weathering resistance and incompatibility with conventional building elements diminish its usability in construction.

With the aim of enhancing the use of bamboo in construction, improving its structural predictability and transforming its vernacular image into a more industrialised one, several research projects on hybrid building systems and engineered bamboo products (EBPs) have been conducted (Trujillo & Archila 2016). Particularly for EBPs using Guadua, Correal *et al.* 2014 characterised the physical and mechanical properties of glue-laminated Guadua (GLG) elements. Their mean values for density and modulus of elasticity (MOE) and ultimate strength in compression parallel to the grain of GLG were 740 kg/m^3, 32.27GPa and 62MPa, respectively. On the basis of these results, (Varela et al. 2013) assessed the seismic performance of a wall-sheathing system using wood for the frame and GLG for the walls. Pinilla & Takeuchi-Tam 2012 manufactured solid and sandwich GLG panels, together with T section beams; whilst Luna et al. 2014 evaluated structural connections for a housing project using these GLG panels for wall and beam elements. Making use of modified fibre bundles, Luna and Takeuchi 2014 in (CORPOICA 2014) manufactured and tested Guadua scrimber beams (a high density unidirectional material pressed at high temperatures and pressure). They reported mean values for ultimate compressive strength that ranged between 46.6MPa and 54.08MPa depending on the adhesive formulation used. Finally, Osorio-Serna et al. 2010 extracted technical fibres from Guadua stems and tested their mechanical properties independently and as composites in combination with epoxy resin.

Despite the active research in this field, EBPs from Guadua are scarce and require complex manufacturing processes. For instance, fabrication of GLG products results in an energy intensive process due to the machining of round culms into rectangular strips that produces high amounts of waste (de Flander & Rovers 2009; Vogtländer et al. 2010). This process also discards the high-density material at the outside of the stem. On the other hand, extraction of technical fibres of Guadua also involves complicated mechanical and chemical processes that end-up discarding high quantities of the material. Therefore, the development of engineered Guadua products needs to exploit its remarkable features, consider an efficient use of the material through appropriate technology and tackle issues regarding natural variability, irregularity and durability. Research at the University of Bath has devised a manufacturing process using thermo-hydro-mechanical (THM) modification (Archila 2015). These modifications were used as a way of reducing machining, wastage and producing flat Guadua strips (FGS) of controlled thickness and density with improved physical and mechanical properties. Mechanical and physical characterisation of the individual FGS demonstrated an average two-fold increase in density, Young's modulus (Archila et al. 2014) and fibre surface area.

There are significant advantages in cross-laminating these panels to produce products with less mechanical anisotropy and superior surface finish. The results from the individual FGS allowed the prediction of the mean elastic and strength values of cross-laminated Guadua (G-XLam) panels and the simulation of the panel's response to axial compressive load in the longitudinal and transverse directions using finite element (FE) modelling software (Archila et al. 2014). Validation of these results by mechanical testing of G-XLam3 & G-XLam5 panels was undertaken and its results are presented in this paper. The elastic mechanical properties of G-XLam3 & G-XLam5 panels were assessed in an axial compression test along (0º) and across their main direction (90º). Physical (contact) and full field (non-contact) measurement methods were used to track deformation in the elastic region and elastic mechanical properties $E_{C,0}$ and $E_{C,90}$ of both panel configurations were evaluated. Digital image correlation (DIC) method was used as the non-contact system to measure strain variations in X, Y (in-plane) and Z axes (out of plane) of the panel surface, whilst linear variable differential transformer (LVDT) transducers were used for the contact system to record deformation along the X axis.

Materials and methods

Two series of in-plane compression tests of G-XLam3 and G-XLam5 panels were undertaken, one series without and another series with buckling restraints. The first series used DIC technique to measure deformation and the second used LVDTs. For both tests series load was kept below the elastic limit and the same panel specimens were used. However, their dimensions varied: G-XLam3 and G-XLam5 panels for the compression test using DIC were 700mm x 700mm, whilst for the compression tests using LVDTs were 600mm x 600mm. Average thickness (t) of the G-XLam3 and G-XLam5 panels was 17.5mm and 27.5mm, respectively.

Restraints were required for panel sizes with a slenderness ratio (λ) over 11 (Bodig & Jayne 1982), as illustrated in Table 1. For the restrained test series, buckling supports presented an obstacle which prevented the capture of full field images of the panel surfaces, thus DIC was not utilized and deformation was measured using LVDTs. For the unrestrained series, deformation was recorded using the DIC technique and buckling failure was avoided; λ was calculated as expressed in equation 1.

$$\boldsymbol{\lambda} = \frac{\boldsymbol{l}}{\boldsymbol{R_g}} \qquad 1$$

where

l is the length of the column and

R_g is the two-dimensional radius of gyration and is defined as the square root of the ratio of second moment of inertia (I) to the cross sectional area (A).

Table 1 compares the slenderness ratio of the G-XLam3 600x600mm and 700x700mm panels. The distribution of cross sectional area (A) around the G-XLam3 panel's centroid axis or radius of gyration (R_g) was almost the same for both panel sizes. Likewise R_g is almost the same for the 600x600mm and 700x700mm size G-XLam5 panels.

The panels were tested in the X_1 (longitudinal) and X_2 (transverse) directions as shown in Figure 1. Two mild steel angle sections were bolted to the top and bottom of the panels to provide vertical alignment and anchorage to the test machine (item 9 in Figure 4) Compression tests of the panels were carried out at a rate of 0.5mm/min in a hydraulic universal test machine.

The resulting engineering strain (Ɛ) from the compression tests was then calculated as the change in length ΔL per unit of original length L, as expressed in equation (2).

$$\varepsilon = \frac{(\Delta \mathrm{L})}{(\mathrm{L})} = \frac{(l_1 - l_0)}{(l_0)} \qquad 2$$

where l_0 is the initial length of the extensometer and l_1 its final length.

Load-strain responses from the load cycles of G-XLam3 & 5 panels were obtained. For both, LVDT and DIC testing methods, the normal stress-strain response of each panel was plotted

(Figure 2a), and a linear regression analysis was performed (Figure 2b). The initial part of these graphs that showed 'parasitic effects' associated with slipping of the test fixture or embedment of the bolts used, were discarded for plotting the stress-strain response of the panels.

Mean values for stress and strain obtained from the longest linear portion of the graph between $0.1F_{max}$ and $0.4F_{max}$ were input into Equation (3) to determine the compression moduli of elasticity (MOE) of the panels in the longitudinal ($E_{C,0}$) and transverse ($E_{C,90}$) directions. The maximum permitted load (F_{max}) and elastic limit were determined from preliminary compression test with a control specimen.

$$E_C = \frac{(F_2 - F_1)l}{(u_2 - u_1)A} \tag{3}$$

where $F_2 - F_1$ is the increment of load between $0.1F_{max}$ and $0.4F_{max}$; $u_2 - u_1$ is the increment of engineering strain corresponding to $F_2 - F_1$; l is the gauge length (A-B length of the virtual extensometer) and A is the cross-sectional area of the panel.

Compression test using DIC

DIC was used to produce an overall picture of deformation of G-XLam3 and G-XLam5 panels and carry out strain measurements on their surface when subjected to in-plane compression load. Two monochrome high-speed cameras (Fast Cam SA3, items 2 and 3 in Figure 3) fitted with Nikon 24-85mm lenses (AF-D Nikkor f/2.8-4) recorded simultaneous images of the speckle pattern painted on the surface of the G-XLam panel (item 1 in Figure 4) at a rate of one frame per second. Both cameras were mounted on a tripod rail that was parallel to the panel and positioned at a stereo angle below 60º (item 7 in Figure 3). Adjustable LED ring lamps fixed to the lenses provided additional illumination (item 11 in Figure 3). Sharp focus, adequate illumination and correct brightness were controlled on screen with the aid of the recording software Photron FASTCAM. A monitor displaying load and stroke readings (item 4 in Figure 3) from the test machine was positioned on one of the camera's field of view.

Prior to test, a calibration grid with 12mm dots spaced at 34.93mm (item 10 in Figure 3) that covered the full field of view was gently moved in front of the panel and sets of approximately 60 images were recorded. Rotation about all three axes permitted the calibration of the stereo-vision system. These images were then analysed using the calibration tool of the VIC3D-2009 software and a low overall error (standard deviation of residuals) for all views ($e \leq 0.015$ –given by the software (Correlated Solutions 2010)) was ensured before running the test. Both recording and analysing software was installed on a laptop with sufficient processing and storage capacity. A reference image was taken once the calibration was performed and before the application of load.

The panels were loaded five times below the elastic limit and buckling failure was avoided. During testing, master and slave cameras captured consecutive images of the full field of view, the increase in load from a monitor (Item 7 in Figure 4) placed to one side, and the corresponding deformations in the X, Y (in-plane) and Z (out of plane) axes of the panel.

It was then possible to track both load and strain for each pair of captured images. These sets of paired images were analysed using VIC3D-2009 software and 2D and 3D strain maps (Figure 5) of the pre-defined area of interest (AOI, item 8 in Figure 4) were produced. Regions with spikes or noise were avoided and a subset value of 21 (size of the tracking grid of points) and step size of five pixels (distance between the points tracked by the software) was chosen for the DIC analysis. Resulting strain in X, Y and Z was calculated by the VIC-3D software.

Using VIC3D-2009 software a virtual extensometer (A-B) was placed at mid-point and mid-height of the reference image of each G-XLam panel (Figure 5a & b) and the axial strain variation for all the captured images was calculated. Typical stress-strain response was plotted for both panels and orientations, and a linear regression analysis was performed for each configuration.

Compression test using LVDT

In-plane compression test using LVDTs and buckling restrains was undertaken on three and five layers G-XLam panels and results were compared with those obtained using the DIC technique. Compressive load was applied to two G-XLam (one G-XLam3 and one G-XLam5) panels with a

2,000kN DARTEC universal test machine (Figure 6) at a rate of 0.5mm/min.

Each panel was tested in the longitudinal (X_1) and transverse (X_2) directions (Figure 6b & c) and was fixed to the testing machine using the fixture shown in Figure 6a (item 2). Buckling restraints with Teflon attached to the specimen and wooden blocks were placed vertically (item 3 in Figure 6) and deformation at 0º, 45º and -45º of the load application axis was measured by LVDTs (item A, B, C and D in Figure 6). LVDTs A, B and C measured displacement variations from zero up to 25mm, while LVDT D had a maximum range of 100mm. Deformation was recorded by a Vishay 5,000 data logger. Data from seven load cycles for each panel configuration and test direction were collated and load-deformation was plotted following the same procedure as with the DIC testing method. A linear regression analysis was performed for each load cycle and the straight part of these graphs between 0.1F_{max} and 0.4F_{max} (elastic region) were input into Equation (3) to determine the longitudinal (L) and transverse (T) moduli of elasticity, MOE (L=$Ep_{C,0}$ and T=$Ep_{C,90}$) of G-XLam3 and G-XLam5 panels.

Results and Discussion

Determination of E_0 and E_{90} of G-XLam panels by compression test using DIC.

Engineering strain values obtained from the virtual extensometer placed (A-B) on G-XLam3 and G-XLam5 panels were used for the calculation of modulus of elasticity in compression in both transverse (X_2) and longitudinal (X_1) orientations ($E_{C,90}$ and $E_{C,0}$, respectively).

$E_{C,0}$ and $E_{C,90}$ results for G-XLam3 and G-XLam5 are presented in Table 2. As can be observed in this table, mean MOE values for both panels in the transverse direction ($Ep_{C,90}$) are considerably lower and present high coefficients of variation (CoV). This can be attributed to the significant slenderness ratio (λ) of the panels that caused rapid out of plane deformation (buckling) and forced the test to be stopped at low load levels. As a result, strain results from the DIC analysis experienced high scatter. The effect of buckling was critical for the G-XLam3 panels tested in the transverse direction (X_2), which resulted in an extremely low value of $Ep_{C,90}$ (mean=2.43GPa). Although, $Ep_{C,90}$ results for G-XLam5 panels presented a considerably higher dispersion of values around the mean (CoV~44%), the buckling effect was minor due to the reduced slenderness ratio, λ=89 for G-XLam3 while for G-XLam5 λ=147.

Out of plane deformation was recorded by the stereovision cameras and analysed using the DIC method producing 3D strain maps for each panel configuration (Figure 7). Manufacturing imperfections were observed using the DIC; however, these surface defects did not exceed ±2mm in-plane (measured linearly on the z axis). Maximum in-plane compression load applied to G-XLam3 and G-XLam5 panels along the longitudinal direction (X_1) was seven and four times the load applied transversely, respectively. This allowed small out of plane deflections without failure.

Strain results from one of the G-XLam3 panel specimens tested in in-plane compression and failed in buckling were discarded for the calculation of the MOE. Figure 8 illustrates this failure and indicates the presence of gaps that triggered the failure.

Determination of E_0 and E_{90} of G-XLam panels by compression test using LVDT.

Global compressive deformation of the G-XLam panels recorded from LVDT-D was used for calculating strain and equation (3) for the calculation of the $Ep_{C,0}$ and $Ep_{C,90}$; results are presented in Table 3.

Deformation recorded from LVDT A positioned at the centre mid-height point of the panels was not representative for calculating the axial strain of the panel during the compression test. Recorded mean values from LVDTs A, B and C, were neglected as values obtained for deformation (δ) oscillated between one and ten microns ($0.01mm > \delta \leq 0.001mm = 1$ micron), which were below the precision range of the LVDTs (±0.025mm for the 25mm and ±0.2mm for the 100mm range LVDT) and resulted in extremely small strains and hence very large MOE values. This was due to the reduced area in which the axial deformation was recorded that did not experience significant deformation (as observed during compression test using DIC) and the increased stiffness of the panel resulting from the use of buckling restraints. During data analysis, misalignment and embedment effects were accounted for and the linear elastic region of the test was used for the calculation of $Ep_{C,0}$ and $Ep_{C,90}$.

Results from in-plane compression tests of G-XLam panels 3 & 5 using DIC and LVDT are presented in Table 4 together with predicted and FE values reported in (Archila et al. 2014). These values have been updated for the conditions of the tests described in this paper. $E_{C,0}$ and $E_{C,90}$ depend on the number of layers and the stiffness's of the individual layers (i.e. E_L and E_T in (Archila et al. 2014)).

Independently of the method used (DIC, LVDT or Analytical), mean values of elastic properties in longitudinal compression ($Ep_{C,0}$) are about 50% and 70% higher than mean elastic properties measured in the transverse direction ($Ep_{C,90}$) for G-XLam3 and G-XLam5 panels, respectively. In spite of the considerably low mean value for $Ep_{C,90}$ obtained from the DIC test of G-XLam3 panels, in general DIC values were higher than the analytical predictions and test results using LVDT. This can be attributed to the significant slenderness ratio (λ) of the G-XLam3 panels that caused rapid out of plane deformation (buckling) and forced the test to be stopped at low load levels (no restrains were used on DIC specimens). As a result, strain values from the DIC analysis experienced high scatter. The effect of buckling was critical for the G-XLam3 panels tested in the transverse direction, which resulted in an extremely low value of $Ep_{C,90}$ (2.43GPa). Although, $Ep_{C,90}$ results for G-XLam5 panels presented a considerably higher dispersion of values around the mean (CoV~44%), the buckling effect was minor due to the reduced slenderness ratio, i.e. λ=89 for G-XLam3 and λ=147 for G-XLam5. Additionally, test with DIC resulted on high variability of results; coefficients of variation (CoV) for the compression test values reached up to 44%. Analytical values provided a reasonably accurate prediction of the elastic properties of G-XLam3 and G-XLam5 panels. Variability of the predicted compressive modulus ($Ep_{C,0}$ and $Ep_{C,90}$) of both panel configurations was below 7%, when compared to the mean tests results using physical measurement systems (LVDT). No permanent deformation (post-test) in any axis was recorded by the DIC; however, 3D strain maps showed areas prone to deformation in the X_3 (R) direction that presented gaps or fabrication defects.

Overall, adequate match between the predictions and the test results using physical (contact) measurement techniques was found for assessing the elastic properties of the panels. By contrast, mean elastic values obtained by the DIC method were considerably higher and presented a considerable scatter of results (CoV). Although it was not the case for all the images, this can be improved in future tests by selecting a larger subset. This can reduce the variation and ‘noise’ seen in some pictures (black holes); nevertheless, the ultimate results will be similar to the obtained values. Differences amongst the results were most likely caused by manufacture flaws and thickness variation within the individual lamellas as seen in Figure 9; unfortunately, their influence could not be statistically determined due to the use of only one test specimen per panel configuration (G-XLam3 and G-XLam5). However, simulations undertaken through finite elements (FE) analysis showed that manufacture defects such as the gaps between lamellas in the faces of the panel had a direct effect on the elastic properties predicted (Table 4).

Conclusions

Mechanical properties of the G-XLam panels were calculated using mean elastic values obtained from previous tests of small clear specimens, subsequently characterised through mechanical testing using the digital image correlation (DIC) method and finally validated with a finite element model (FEM). Mean elastic values from DIC for G-XLam3 and G-XLam5 panels were 17.22GPa and 15.67GPa in the main direction ($Ep_{C,0}$) and 2.43GPa and 9.46GPa in the transverse direction ($Ep_{C,90}$). While mean elastic values from LVDTs for G-XLam3 and G-XLam5 panels were 14.86GPa and 12.48GPa in the main direction ($Ep_{C,0}$) and 7.43GPa and 8.74GPa in the transverse direction ($Ep_{C,90}$). As expected, the higher stiffness of G-XLam3 panels along the main direction is due to the proportionally higher ratio of material longitudinally orientated along the loading direction (i.e. 0.66 in G-XLam3 and 0.6 in G-XLam 5 panels). Similar mean MOE values from mechanical testing in longitudinal compression (Ep_0, 5ply = 14 GPa) have been reported by Verma & Chariar 2012 for cross laminated bamboo products using different manufacturing and testing techniques. This research has pioneered the use of DIC techniques for the measurement of deformation on EBPs. However, mean values obtained using this method were higher and presented a higher variability than the analytical predictions and test results using LVDT. Whilst there is a great potential on the use of this type of non-contact measurement methods for remote and non-destructive testing of materials and structures, further testing and improvements to the utilisation of the DIC method in bio-based materials such as EBPs is required. For instance, adjustments on the speckle pattern and the subset size (e.g. a larger subset) might result on a lower coefficient of variation (CoV).

Furthermore, mean results for the mechanical properties of G-XLam panels obtained in this research are higher than the characteristic elastic values of comparable engineered wood products (e.g. CLT panels). Comparison of the LVDT and predicted results for G-XLam panels with those of analogous CLT panels (M1 BSP crossplan by Mayr-Melnhof Holz) show an approximate two-fold increase in density and MOE (Table 4). This is, the in-plane compression moduli of elasticity of these CLT panels in the main direction ($Ep_{C,0}$) and transverse direction ($Ep_{C,90}$) were about half of that of G-XLam panels (e.g. $Ep_{C,0}$ was 7.57GPa and 14.83 GPa for CLT3 and G-XLam3 panels). On the other hand, the thickness of G-XLam3 and G-XLam5 panels is almost a fifth of CLT3 and CLT5 panels (e.g. thicknesses of CLT5 and G-XLam5 were 134mm and 27.5mm, respectively). This is a desirable feature in stiffness driven design but, the high slenderness of G-XLam elements present a structural challenge in overcoming buckling. For instance, potential engineering applications for G-XLam panels are sandwich panels and stressed skin structures (e.g. monocoque), where thin but very stiff layers are separated by a core or internal structure that increases the second moment of area and reduces buckling. This highlights the potential of engineered bamboo products (EBPs) such as G-XLam, as a complementary material (not a substitute) in structural applications combined with wood and/or lightweight cores to provide the required stiffness with a reduced cross-section. However, further testing, research and understanding of the mechanical behaviour of EBPs is required, together with the optimisation of current manufacturing processes and their incorporation within timber standards for structural design. Although there are no standards for EBPs, this research has made use of timber engineering knowledge and standardised methods for engineered wood products, which makes timber standards a feasible framework for the assessment of EBPs.

Acknowledgements

The authors are grateful to Amphibia Group SAS (Colombia), Amphibia BASE Ltd (UK), and COLCIENCIAS, for the financial support provided and to *Grupo de Investigación en Análisis,* *Diseño y Materiales* (GIES) at Universidad Nacional de Colombia (Bogotá) for materials provided and logistical support given during the execution of the research.

References

Archila, H.F. et al., 2014. Evaluation of the mechanical properties of cross laminated bamboo panels by digital image correlation and finite element modelling . In A. J. Salenikovich, ed. *WCTE 2014, World Conference on Timber Engineering*. Quebec, QC: ISBN 978-0-86488-560-9, p. 43.

Archila, H.F., 2015. *Thermo-hydro-mechanically modified cross-laminated Guadua-bamboo panels*. PhD Thesis. University of Bath.

Archila, H.F., Ansell, M.P. & Walker, P., 2012. Low Carbon Construction Using Guadua Bamboo in Colombia. *Key Engineering Materials*, 517, pp.127–134.

Bodig, J. & Jayne, B.A., 1982. *Mechanics of wood and wood composites* Reprint ed., New York, U.S.A.: Van Nostrand Reinhold Company.

CORPOICA, 2014. Consolidando el sector con Innovación y Sostenibilidad. In *II Simposio Internacional Guadua y Bambú*. Bogotá D.C., Colombia: 978-958-716-724-5, p. 224.

Correal, J.F. et al., 2014. Experimental evaluation of physical and mechanical properties of Glued Laminated Guadua angustifolia Kunth. *Construction and Building Materials*, 73, pp.105–112.

Correlated Solutions, 2010. *Vic-3D 2010, testing guide*,

de Flander, K. & Rovers, R., 2009. One laminated bamboo-frame house per hectare per year. *Construction and Building Materials*, 23(1), pp.210–218.

Hidalgo-López, O., 2003. *Bamboo: The gift of the gods* First., Bogotá D.C./Colombia: D’vinni Ltda.

Janssen, J.J.A., 2000. *Designing and Building with Bamboo, INBAR Technical Report No.20* A. Kumar, ed., Eindhoven: INBAR-International Network for Bamboo and Rattan.

Jayanetti, D.L. & Follett, P.R., 1998. *Bamboo in construction, An introduction. INBAR Technical Report No. 15*, UK: TRADA Technology, Ltd.

Kaminski, S., Lawrence, A. & Trujillo, D., 2016. *Design guide for engineered bahareque housing.*, Beijing, China.

van der Lugt, P., Vogtländer, J. & Brezet, H., 2009. *Bamboo , a Sustainable Solution for Western Euope Design Cases , LCAs and Land-use*, Beijing, People's Republic of China & The Netherlands: International Network for Bamboo and Rattan (INBAR) & Delft University of Technology, Faculty of Industrial Design Engineering, Design for Sustainability Program.

Luna, P., Olarte, A.M. & Takeuchi-Tam, C.P., 2014. Análisis teórico experimental de conexiones en elementos estructurales de bambú guadua laminado pegado prensado, para un proyecto de vivienda. *Dyna rev.fac.nac.minas*, 81(184), pp.110–114.

Mayr-Melnhof Kaufmann Group, 2009. *Manual Cross-laminated timber panels M1 BSP cross plan*, Austria.

Minke, G., 2012. *Building with bamboo: design and technology of a sustainable architecture.*, Basel, Switzerland: Walter de Gruyter.

Osorio-Serna, L.R. et al., 2010. The relation between bamboo fibre microstructure and mechanical properties. In *14th European Conference on Composite Materials*. Budapest/Hungary, p. 10.

Pinilla, J.J. & Takeuchi-Tam, C.P., 2012. The structural behaviour of laminated-guadua panels under parallel plane loads. *Ingeniería e Investigación*, 32(2), pp.18–22.

Trujillo, D. & Archila, H.F., 2016. *Engineered bamboo and bamboo engineering*, High Wycombe, Buckinghamshire, HP14 4ND, UK.

Trujillo, D.J.A., Ramage, M. & Chang, W.-S., 2013. Lightly modified bamboo for structural applications. *Construction Materials*, 166(CM4), pp.238–247.

Varela, S. et al., 2013. Cyclic Performance of Glued Laminated Guadua Bamboo-Sheathed Shear Walls. *Journal of Structural Engineering*, 139(11), pp.2028–2037.

Verma, C.S. & Chariar, V.M., 2012. Development of layered laminate bamboo composite and their mechanical properties. *Composites Part B: Engineering*, 43(3), pp.1063–1069.

Villegas, M., 2003. *New Bamboo. Architecture and Design.*, Bogotá D.C./Colombia: Villegas editores.

Vogtländer, J., van der Lugt, P. & Brezet, H., 2010. The sustainability of bamboo products for local and Western European applications. LCAs and land-use. *Journal of Cleaner Production*, 18(13), pp.1260–1269.

Xiao, Y., Inoue, M. & Paudel, S.K., 2008. Modern Bamboo structures. In Y. Xiao, M. Inoue, & S. K. Paudel, eds. *Proceedings of the 1st International Conference on Modern Bamboo Structures (ICBS 2007)*. London/UK: Taylor & Francis Group, pp. 5–21.

List of Figures (images as individual files separate to your MS Word text file).

transverse (X2) direction. d) G-XLam5 panel tested along the longitudinal (X1) direction.

Figure 8. G-XLam3 panel discarded for buckling failure during compression test using DIC. a) Failure of panel mounted on the test machine b) 3D-Strain map of the failure c) Detail of the failure area. d) Detail of the shear failure produced by the buckling effect during compression test.

Figure 9. Thickness variation and gaps across the section of a G-XLam5 panel.

List of Tables

Table 3 Elastic mechanical properties of G-XLam panels obtained from compression test using LVDTs

Specimen	G-XLam3 (L)	G-XLam3 (T)	G-XLam5 (L)	G-XLam5 (T)
Property	$Ep_{C,0}$ (GPa)	$Ep_{C,90}$ (GPa)	$Ep_{C,0}$ (GPa)	$Ep_{C,90}$ (GPa)
Mean	14.86	7.43	12.48	8.74
SD	1.17	0.69	0.92	0.76
CoV	8%	7%	7%	9%

Table 2. MOE results for G-XLam panels using DIC

$E_{C,0,90} = \frac{(F_2 - F_1)l}{(u_2 - u_1)A}$	G-XLam3		G-XLam5	
	$E_{C,0}$ (GPa)	$E_{C,90}$ (GPa)	$E_{C,0}$ (GPa)	$E_{C,90}$ (GPa)
Cycle 1	18.65	2.92	18.53	-
Cycle 2	15.25	3.18	11.42	10.87
Cycle 3	14.20	1.86	14.34	7.24
Cycle 4	15.84	1.64	18.56	5.14
Cycle 5	22.16	2.43	15.67	14.59
Mean	17.22	2.43	15.67	9.46
st dev	3.22	0.66	3.02	4.16
CoV	19%	27%	19%	44%

Table 1. Slenderness ratio of the G-XLam panels tested.

	G-XLam3 (700mm x 700mm)	G-XLam5 (700mm x 700mm)	G-XLam3 (600mm x 600mm)	G-XLam5 (600mm x 600mm)
b (mm)	700	700	600	600
d (mm)	16.5	27.5	16.5	27.5
I (mm^4)	262,040.25	1,213,151.04	224,606.25	1,039,843.75
A (mm^2)	11,550	19,550	9,900	16,500
R_g (mm)	4.76	7.87	4.76	7.93
λ	147	89	126	75

Figure 9. Thickness variation and gaps across the section of a G-XLam5 panel.

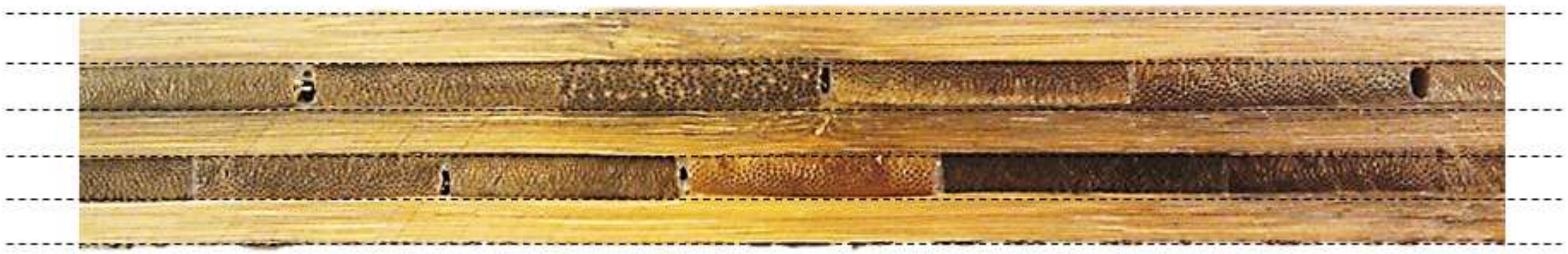

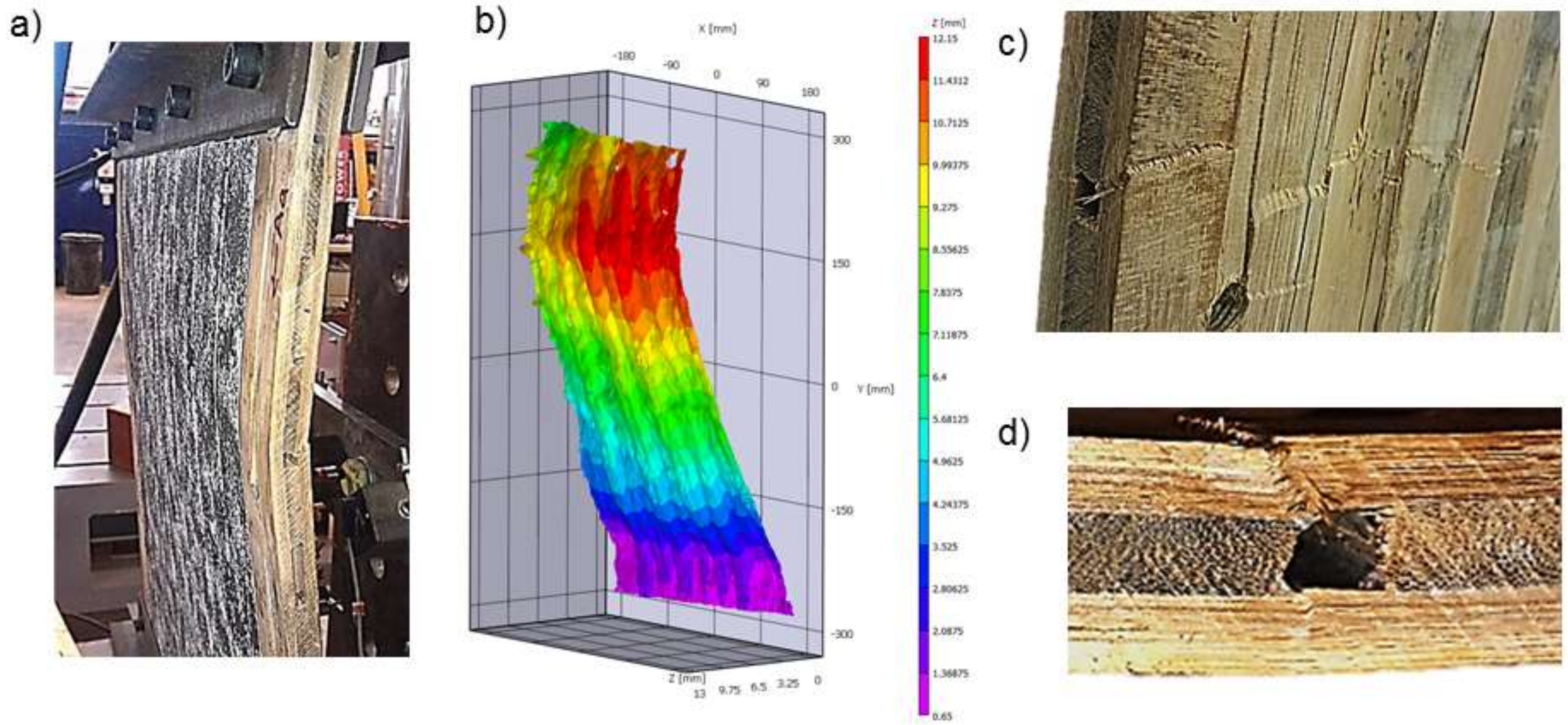

Figure 8. G-XLam3 panel discarded for buckling failure during compression test using DIC. a) Failure of panel mounted on the test machine b) 3D-Strain map of the failure c) Detail of the failure area. d) Detail of the shear failure produced by the buckling effect during compression test.

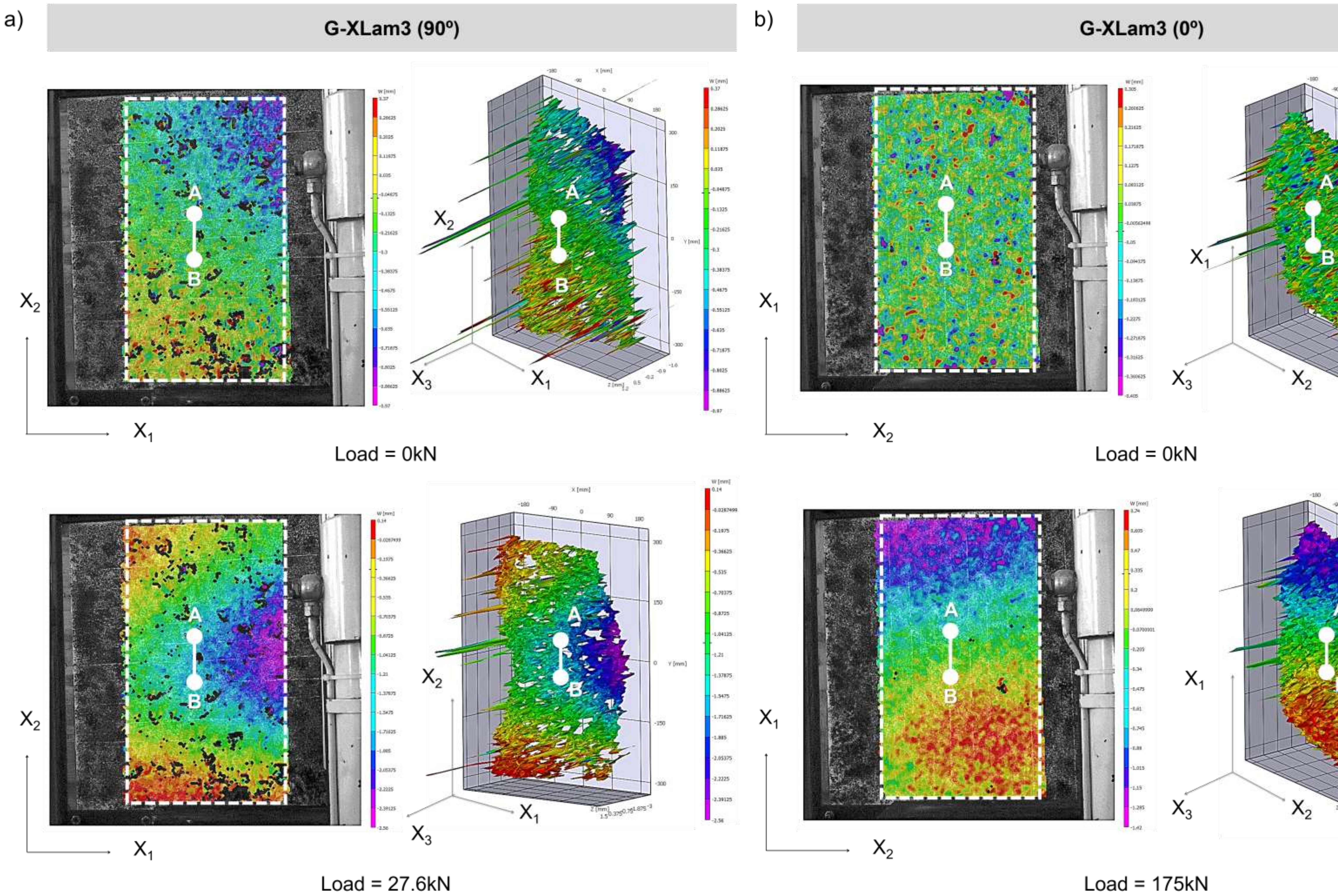

a)
G-XLam3 (90º)
b)
G-XLam3 (0º)
A
B
X_1
X_2
X_3
Load = 0kN
Load = 27.6kN
Load = 0kN
Load = 175kN

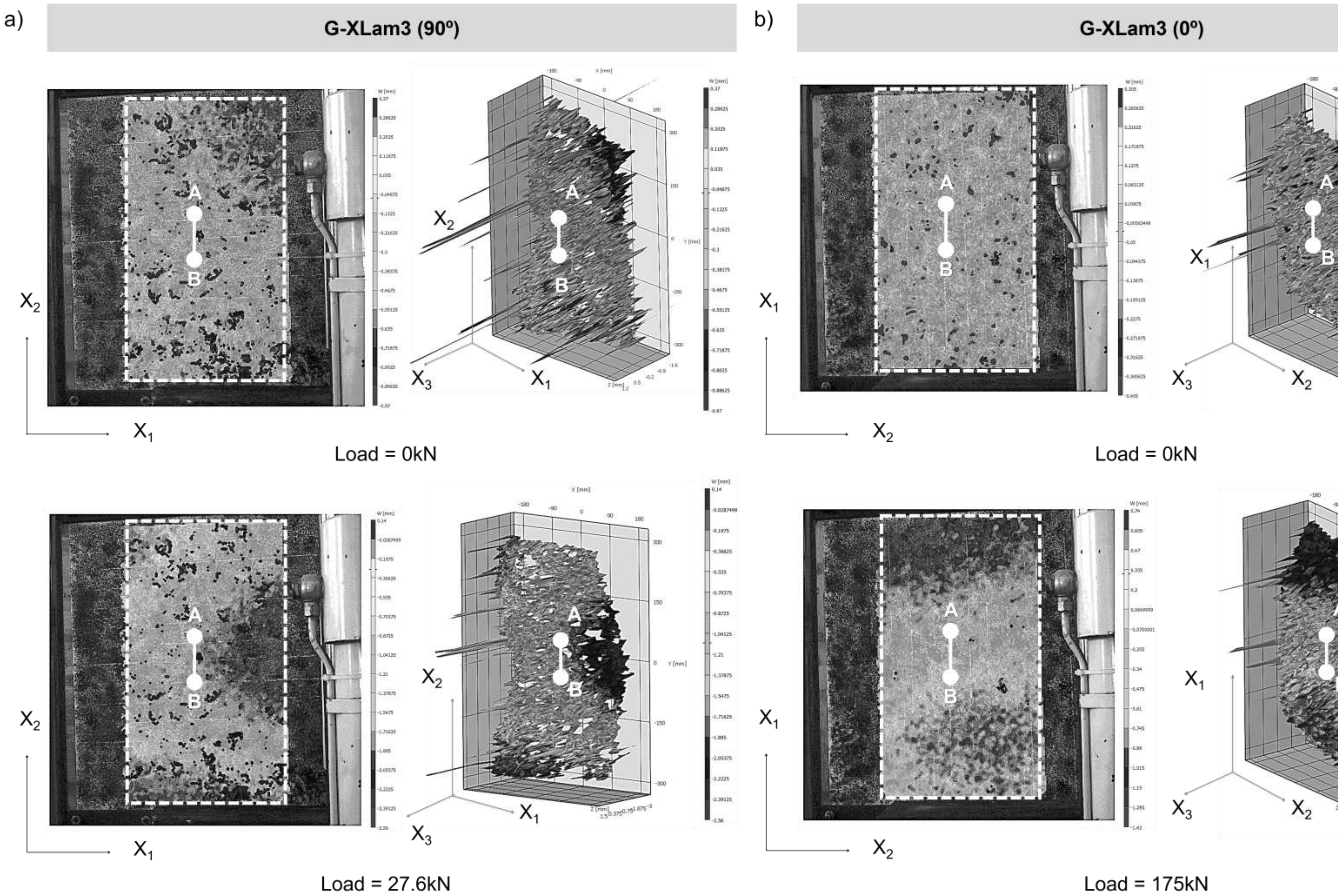

a)
G-XLam3 (90º)
b)
G-XLam3 (0º)
A
B
X2
X1
X3
Load = 0kN
Load = 0kN
Load = 27.6kN
Load = 175kN

a)

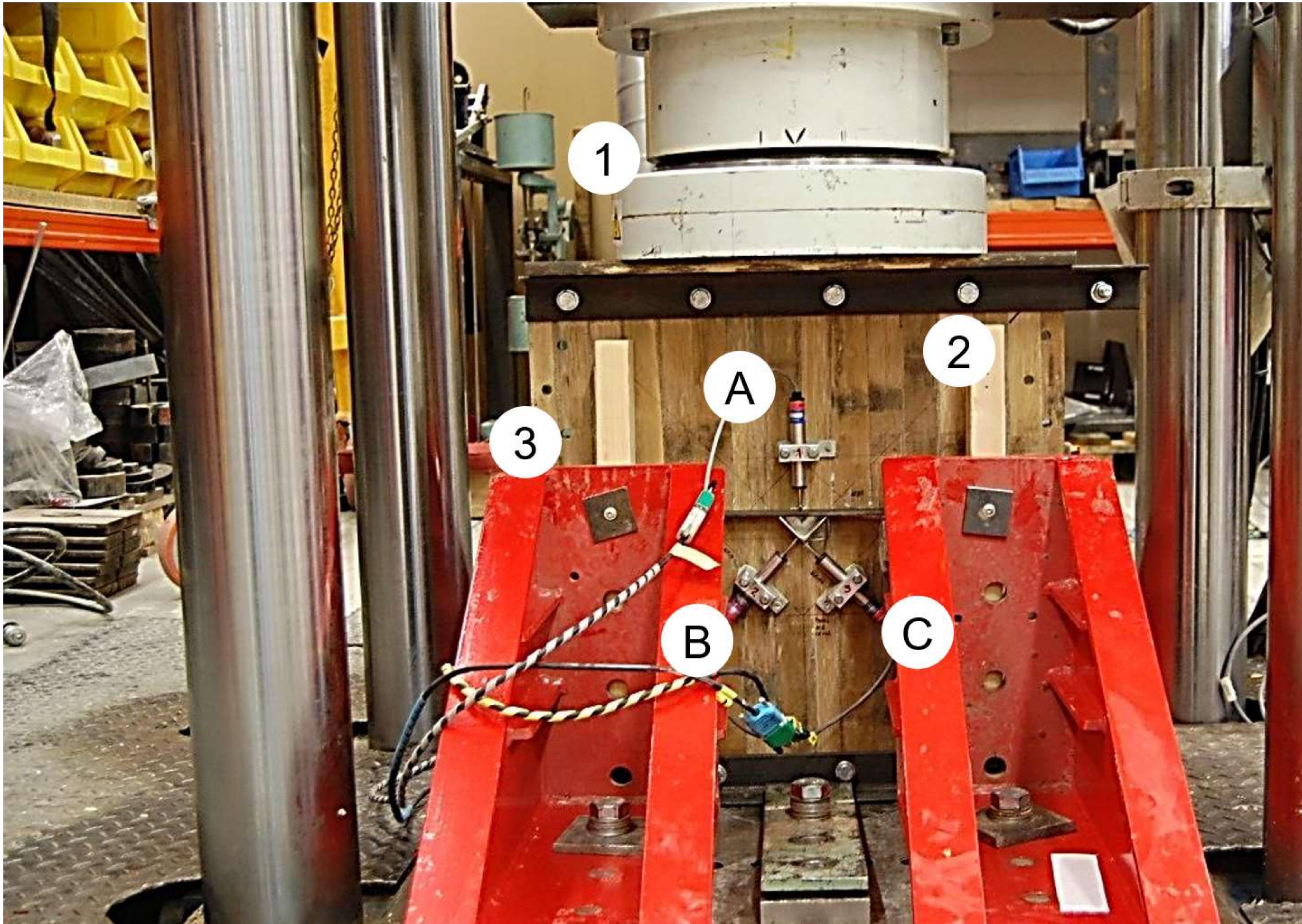

Figure 5. a) Strain map in X_3 (radial) direction of a G-XLam panel tested in compression along X_2 (transverse) axis.

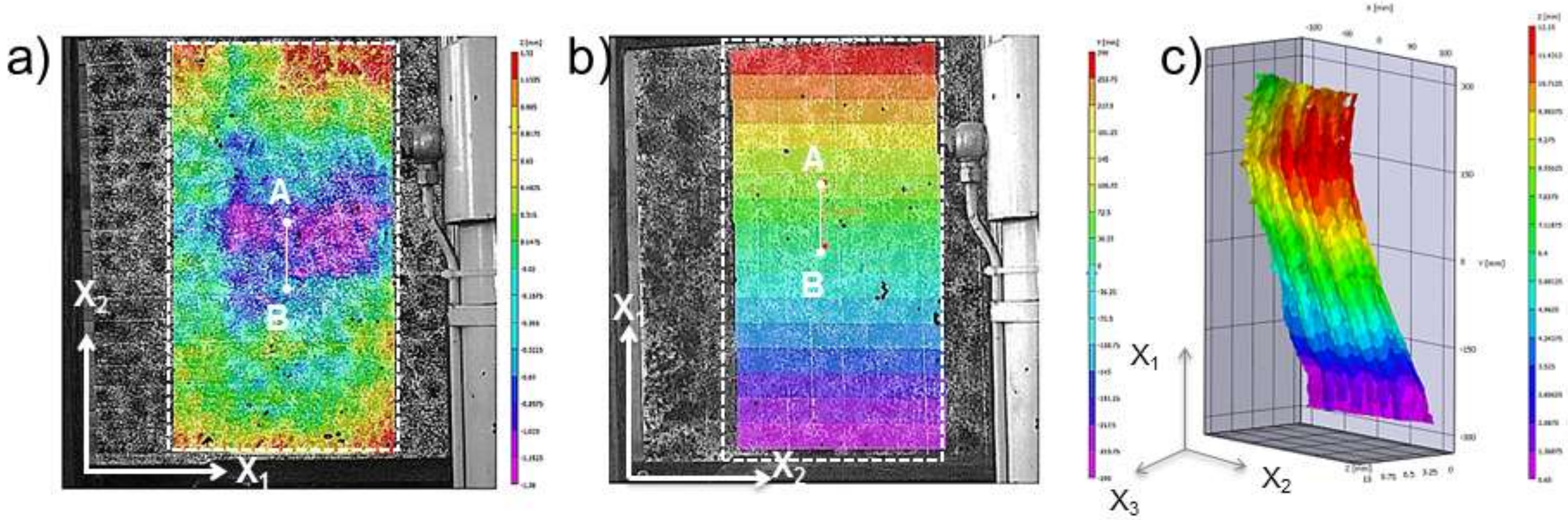

Figure 4. Setup for the compression test of CLG panels using the DIC method.

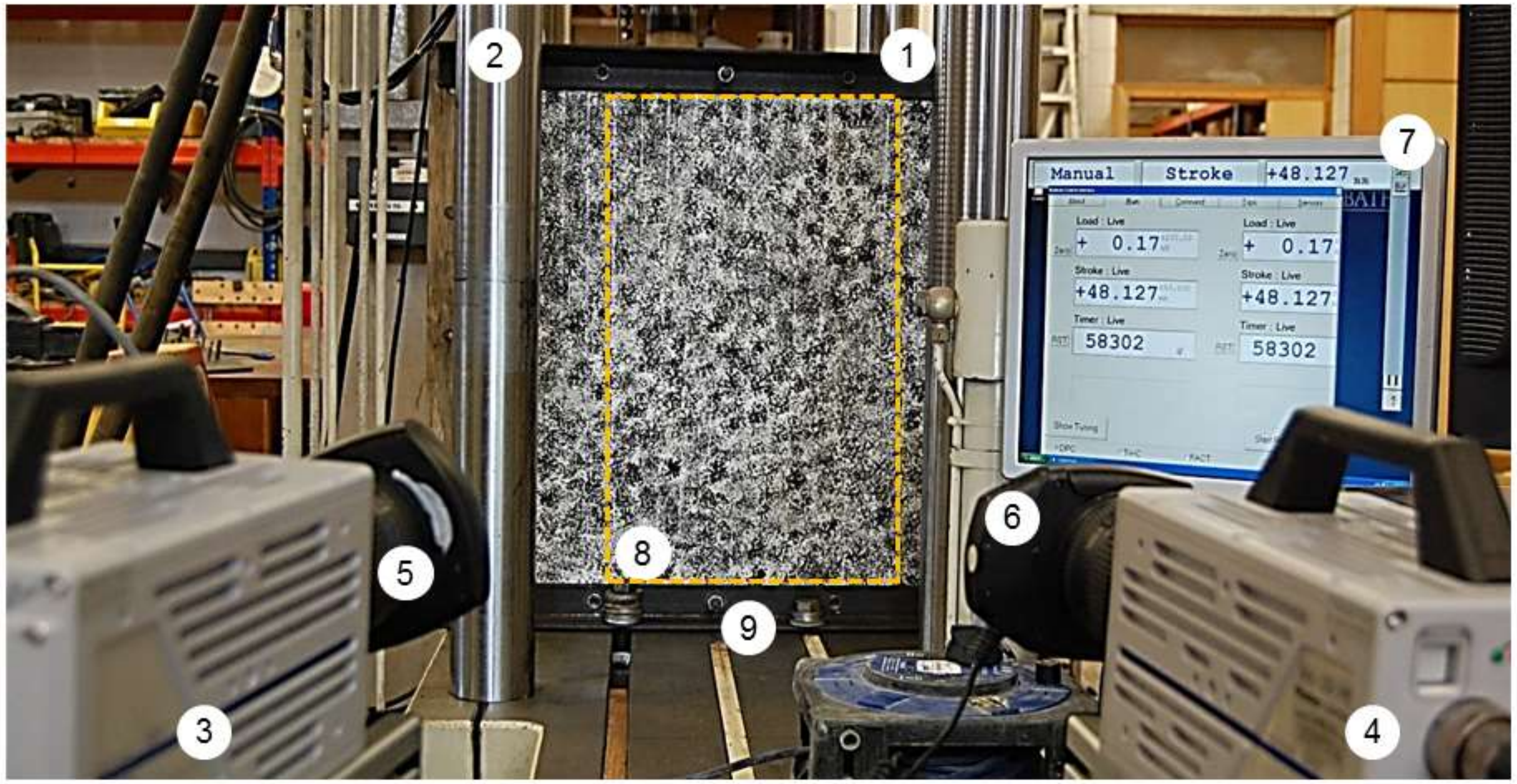

1. Object: G-XLam panel. 2. Mayes 20kN test machine. 3. Master camera. 4. Slave camera.
5. Nikon lenses 24-85mm. 6. LED lighting. 7. Load display: Monitor. 8. Area of interest.
9. Angle sections

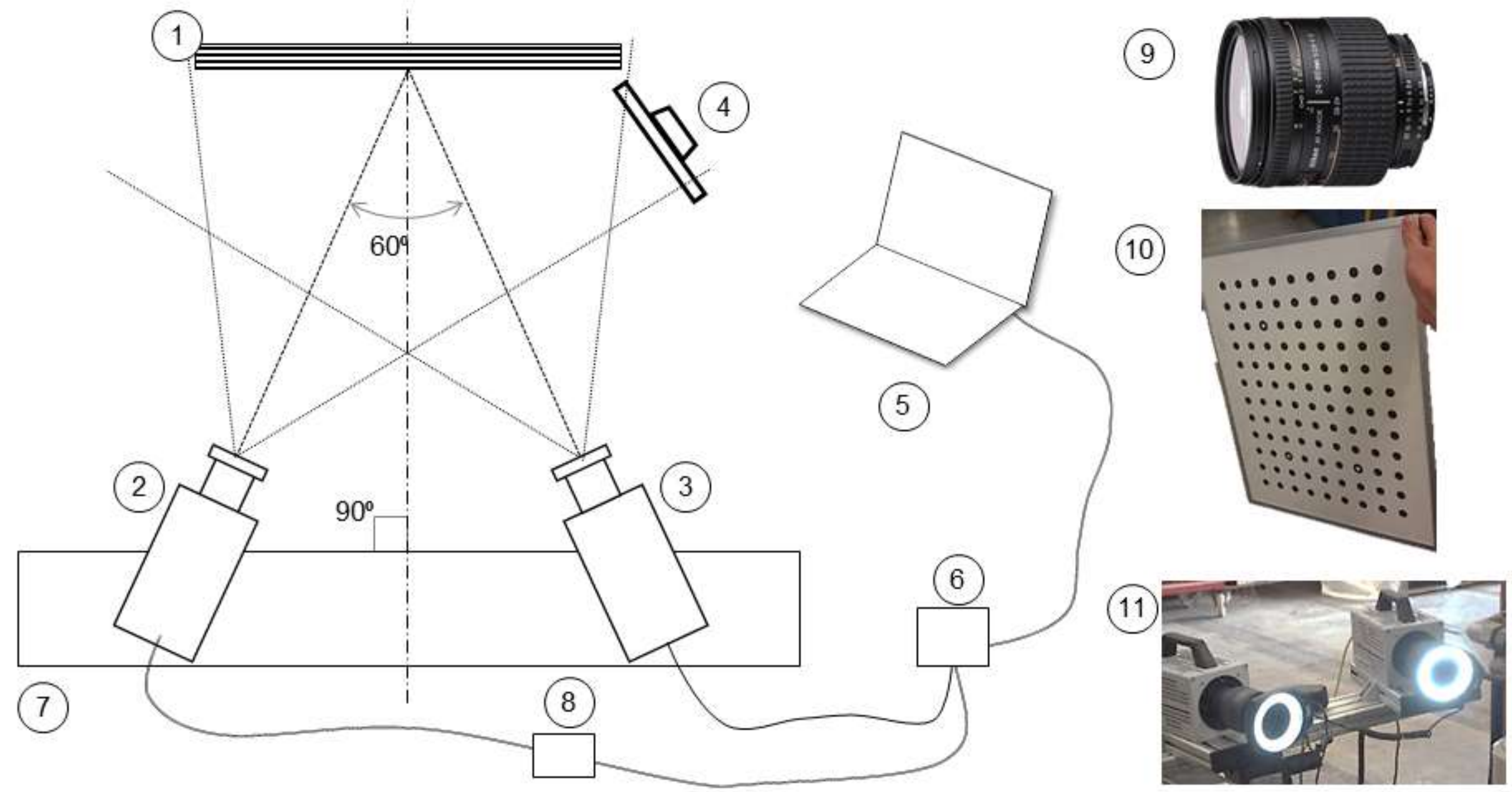

1. Object: G-XLam panel. 2. Master camera. 3. Slave camera. 4. Load display: Monitor.
5. Laptop. 6. Router. 7. Tripod rail. 8. Remote shutter switch.
9. Nikon lenses 24-85mm. 10. Calibration grid. 11. LED lighting

Figure 3 DIC test configuration and instrumentation.

Figure 2. a) Compressive load versus compressive strain (DIC) data obtained from in-plane compression tests on the G-XLam5 panel tested along the longitudinal, X_1 axis. b) Average load versus strain graph derived from the DIC data.

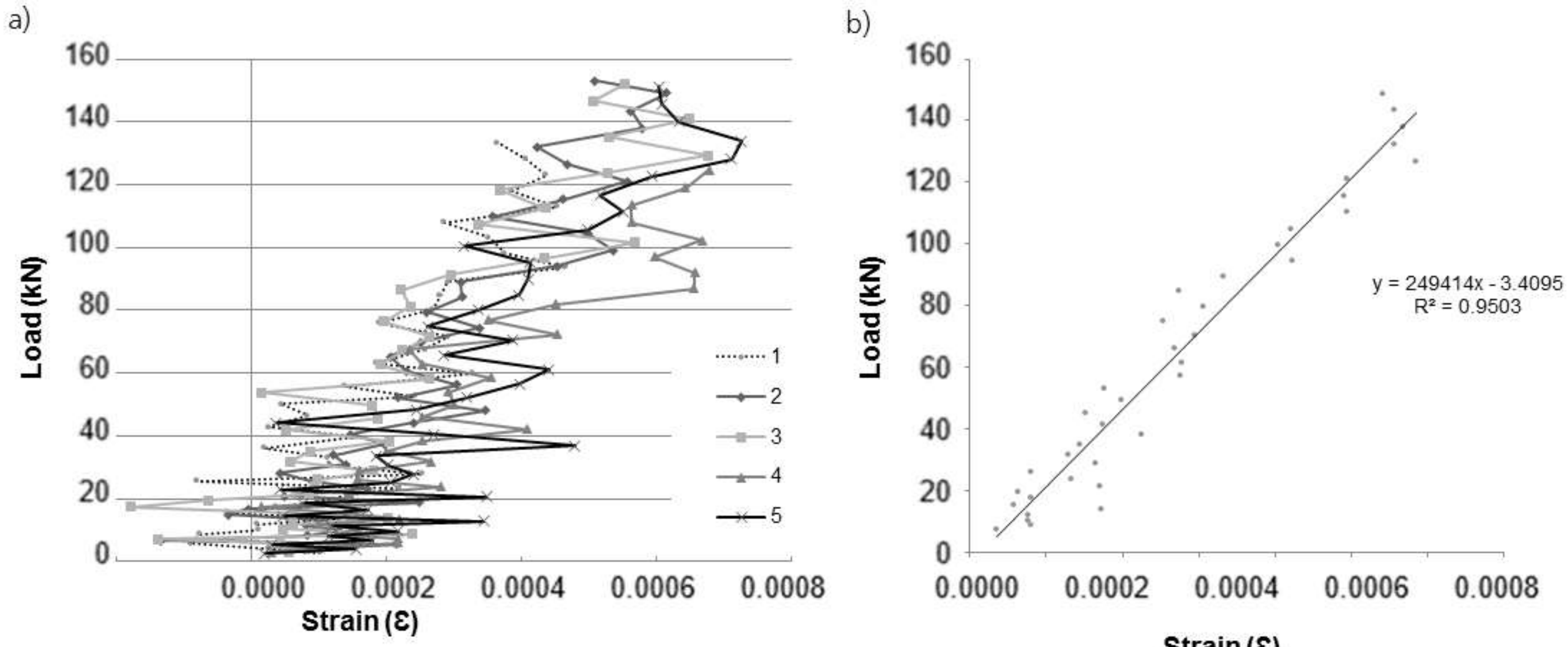

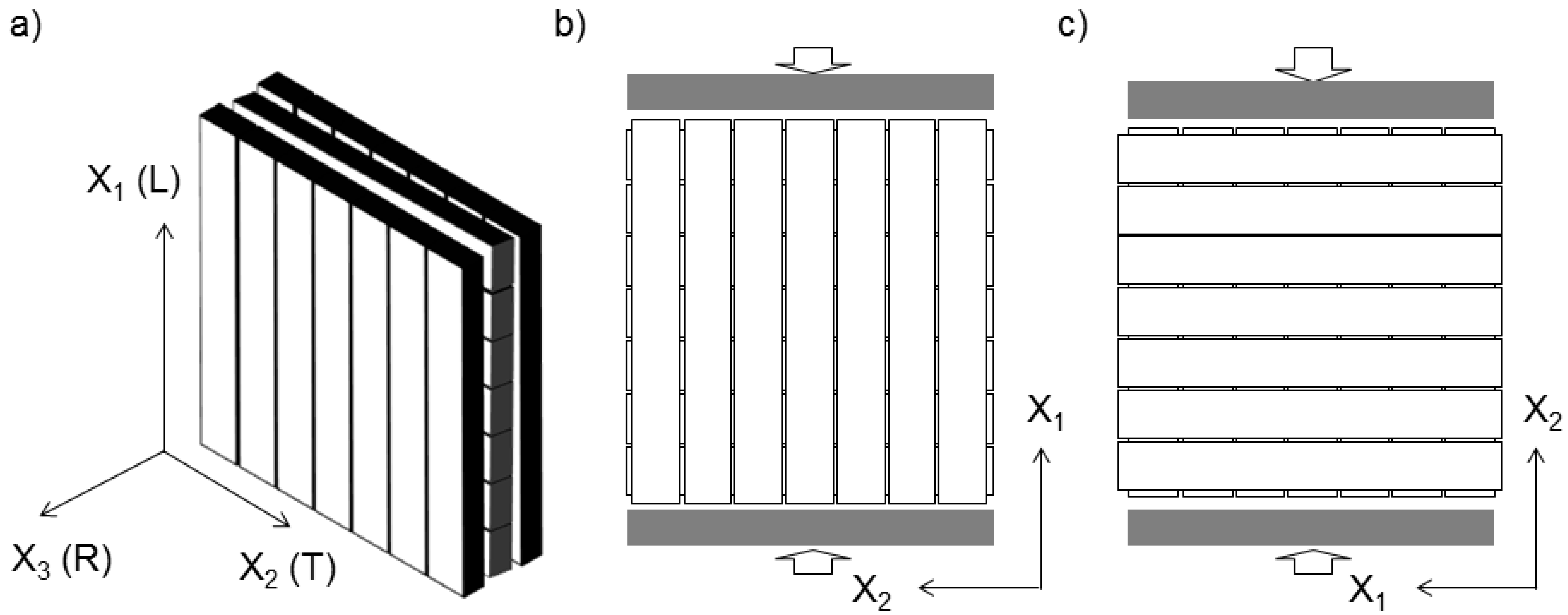

Figure 1 a) Geometric (X_1, X_2, X_3) and orthotropic (L, T, R) axis of the G-XLam panels b) Diagram of the compression test in the longitudinal direction of the panel c) Diagram of the compression test in the transverse direction of the panel.

Table 4 Summary of the results obtained from the in-plane compression panel testing and the FE and predicted values previously obtained by (Archila et al. 2014).

	G-XLam3 (t=17.5mm; ρ=890 kg/m^3)		G-XLam5 (t=27.5mm; ρ=890 kg/m^3)	
	$E_{C,0}$ (GPa)	$E_{C,90}$ (GPa)	$E_{C,0}$ (GPa)	$E_{C,90}$ (GPa)
DIC-test	17.22	2.43	15.67	9.46
st dev	3.22	0.66	3.02	4.16
CoV	19%	27%	19%	44%
LVDT-test	14.86	7.43	12.48	8.74
SD	1.17	0.69	0.92	0.76
CoV	8%	7%	7%	9%
Predicted	14.83	7.93	13.45	9.31
FEM (gapless)	20.69	10.75	18.70	12.66
FEM (with gaps)	18.75	9.56	16.94	11.42
CLT M1 BSP crossplan (Predicted)*	CLT 3 (t=78mm; ρ~480 kg/m^3)		CLT 5 (t=134mm; ρ~480 kg/m^3)	
	7.57	3.91	6.74	4.62